Science Advances
AAAS

advances.sciencemag.org/cgi/content/full/5/10/eaax4961/DC1

Supplementary Materials for

Stretchable elastic synaptic transistors for neurologically integrated soft engineering systems

Hyunseok Shim, Kyoseung Sim, Faheem Ershad, Pinyi Yang, Anish Thukral, Zhoulyu Rao, Hae-Jin Kim, Yanghui Liu, Xu Wang, Guoying Gu, Li Gao, Xinran Wang, Yang Chai, Cunjiang Yu*

*Corresponding author. Email: cyu15@uh.edu

Published 11 October 2019, *Sci. Adv.* **5**, eaax4961 (2019)
DOI: 10.1126/sciadv.aax4961

This PDF file includes:

Calculation of mobility and threshold voltage

The field effect mobilities were obtained from the output current versus voltage in the saturation region. In this regime, we fitted the plot of the $\sqrt{I_{DS}}$ versus V_{gs} and extracted the mobilities based on following equation

$$I_{ds} = \left(\frac{WC_i}{2L}\right)\mu_{FE}(V_{gs} - V_{th})^2 \quad \text{(S1)}$$

where L, W, and C_i are the channel length, the width, and the gate capacitance per unit area, respectively. The x-intercept of the extrapolation of the fitted curve define the threshold voltage (V_{th}).

Fabrication of deformable neurologically integrated tactile sensory skin

The fabrication for the stretchable tactile sensory skin started with the fabrication of transistor array followed the procedure for the individual synaptic transistor as described in Materials and Methods. The backside of the rubbery synaptic transistor array was placed on a pressure sensitive rubber sheet (ZL45.1, Zoflex). Conductive rubber paste was used to connect the transistor gate and rubber sheet, which was solidified at 50 °C for 5 hours. PDMS (10:1, prepolymer/curing agent) was spin coated on the rubbery synaptic transistor array as an encapsulation layer. Finally, the rubbery synaptic transistor array with pressure sensitive rubber sheet was laminated onto an elastic sheet with patterned gated electrodes to complete the tactile sensory skin.

Design and fabrication of the soft pneumatic robot

The design of the soft pneumatic robot (SPR) employs the large deformation capability of silicone elastomer. The SPR consists of two identical rectangular-shape pneumatic actuators (RPAs). Each RPA contains the main body part and the end cap part. The geometry parameters of the two parts are shown in fig. S16. The two RPAs are arranged side by side and winded with the much stiffer fibers. The fibers serve to limit the excessive radial expansion of the RPAs while preserve the axial extension of the RPAs. The SPR can realize straight walking and bi-directional steering movements with the cooperation of its two RPAs (see Fig. 5F). While the RPA on the left and the RPA on the right are inflated with the same pressure simultaneously, the two RPAs generate same amount of axial extension and the SPR realize straight walking motion. When the left RPA is inflated and the right RPA is deflated, the left side of the SPR achieves axial extension while the right side does not. Therefore, the SPR bends to right side and realizes right turn movement. Similarly, the SPR can also realize left turn movement.

The SPR was fabricated by first casting the RPAs, then assembling the RPAs and finally winding the fibers. Specifically, the RPAs were fabricated using the molding approach (*46-49*). Molds were designed for the main bodies and end caps of the RPAs. All the molds were 3-D printed. Commercial silicone elastomer M4601 (Wacker) was employed to cast the RPAs. The component A and component B of the elastomer were mixed by mass ratio of 9:1 and degassed before casting. In the casting process, the release agent was first sprayed on the surfaces of the molds for ease of demolding. The mixed elastomer was the gently injected into the molds. The filled molds were then placed in the oven at 70 °C until the elastomer is cured. After demolding,

the casted end caps were inserted into the main bodies to form the complete RPAs. The interfaces of the end caps and the main bodies were sealed with the liquid elastomer. Subsequently, the RPAs were placed into the oven at 70 °C to solidify. To form one SPR, two RPAs were arranged side by side. The RPAs were winded with fibers. After winding, the fabrication of the SPR is completed. The end caps of the two RPAs connect the tubing for pneumatic actuation by air.

Fabrication of robotic skin

The fabrication of the robotic skin with TENGs, resistors, diodes and synaptic transistors started with creating rubbery electrodes based on AgNWs/PDMS as described in Methods. The skin components on top, right, and left sides are identical. Then the processes continued with the fabrication of diodes. One electrodes of the diodes was AuNPs-AgNWs/PDMS, where the AuNPs coating on AgNWs electrodes were created by galvanic replacement. The other is Al-Cr-AgNWs/PDMS, which was accomplished by treating the AgNWs/PDMS with UVO for 10 min, and then sequentially deposit Cr (5 nm) and Al (40 nm). A layer of P3HT-NFs/PDMS was then coated to create diodes, resistors and synaptic transistors. The channel length and width of the synaptic transistors are 60 μm and 2 mm, respectively. The resistor from P3HT-NFs/PDMS is ~110 MΩ. A layer of PDMS was spin coated at 400 rpm for 30 s on the TENG electrode to complete the robotic skin. Finally, the elastic skin was wrapped on soft robot to finalize the soft adaptive neurorobot.

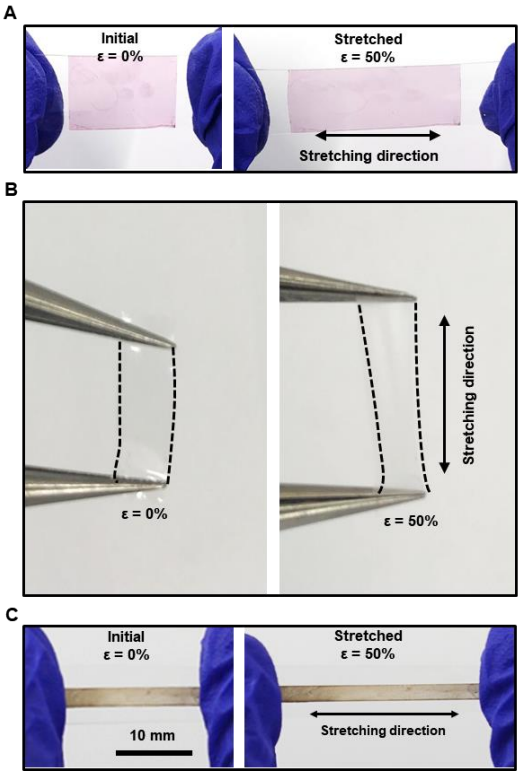

Fig. S1. Optical image of fully rubbery electronic materials. (**A**) P3HT-NFs/PDMS semiconductor on PDMS. (**B**) ion gel dielectric. (**C**) AuNPs-AgNWs/PDMS conductor. (Photo Credit: Hyunseok Shim, University of Houston).

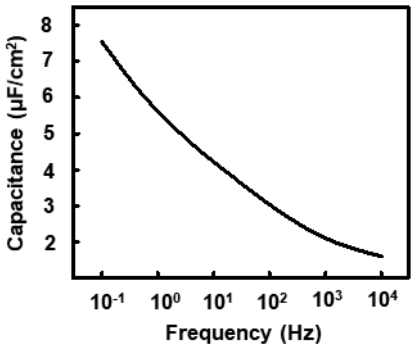

Fig. S2. Frequency-dependent capacitance per unit area.

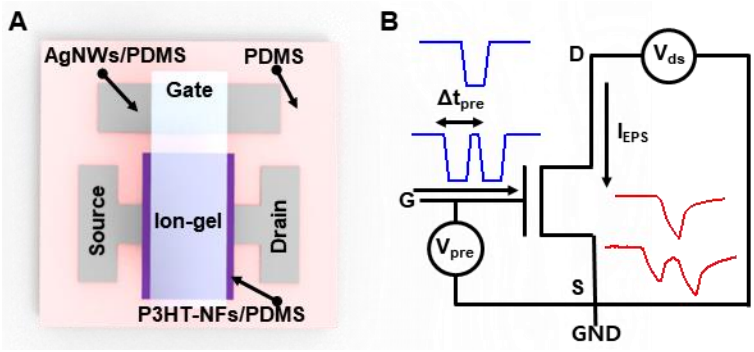

Fig. S3. Schematic information of synaptic transistor. (**A**) Schematic illustration in top view. (**B**) Schematic operational diagram.

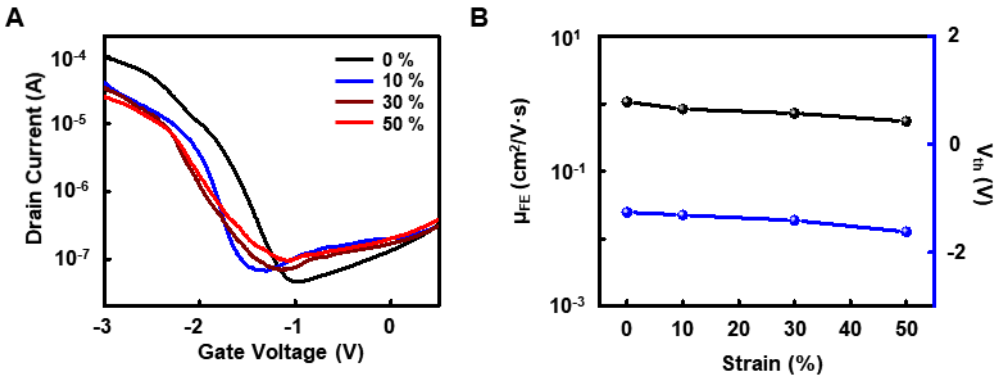

Fig. S4. Transfer curve and mobilities of the rubbery synaptic transistor. (**A**) Transfer curve depending under mechanical strains. (**B**) Mobility and threshold voltage under mechanical strains.

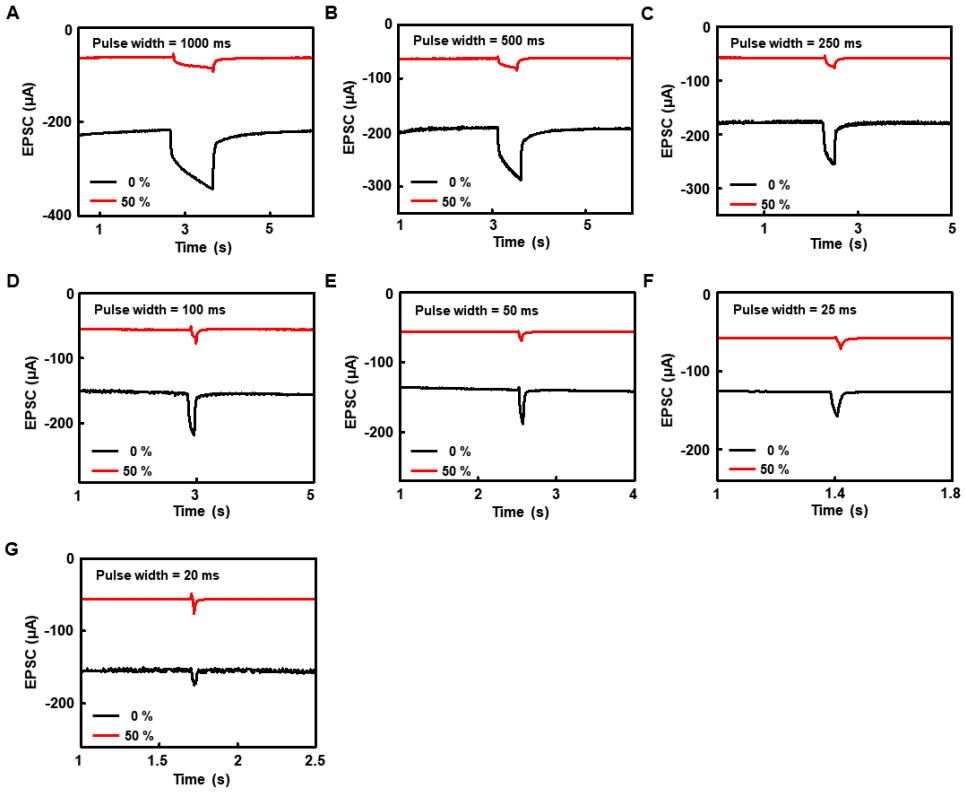

Fig. S5. EPSC results with respect to different pulse widths without (0%) and with 50% strain. (**A**) 1000. (**B**) 500. (**C**) 250. (**D**) 100. (**E**) 50. (**F**) 25. and (**G**) 20 ms.

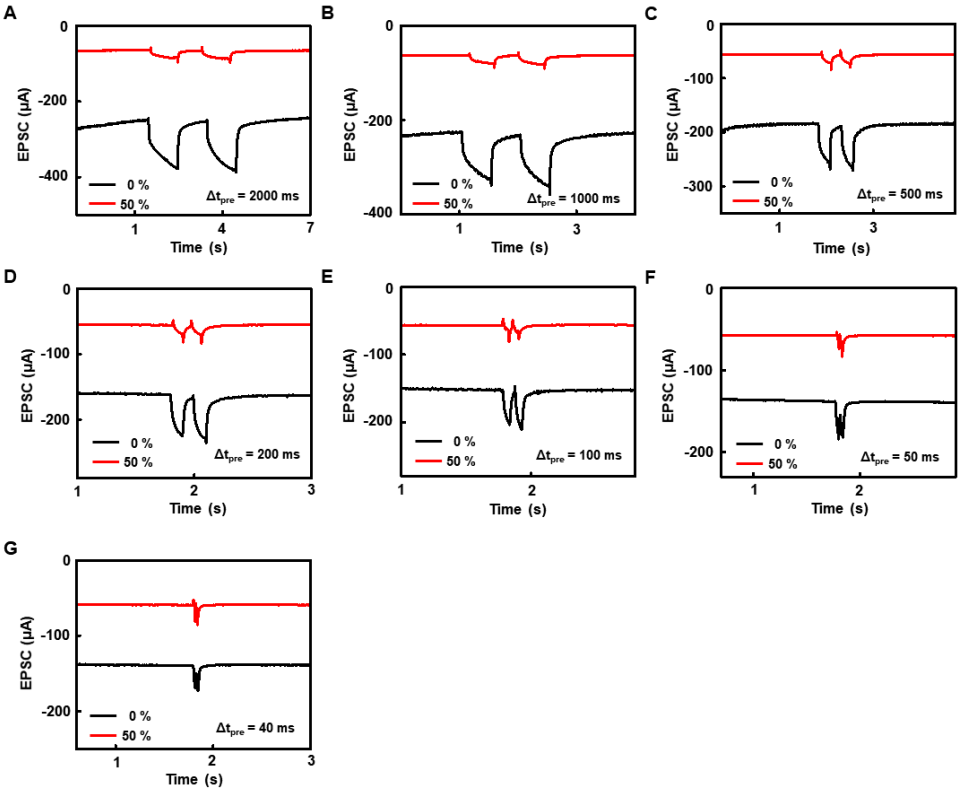

Fig. S6. EPSC results triggered by two successive synaptic pulses with respect to different Δt_{pre} without (0%) and with 50% strain. (**A**) 2000. (**B**) 1000. (**C**) 500. (**D**) 200. (**E**) 100. (**F**) 50. and (**G**) 40 ms.

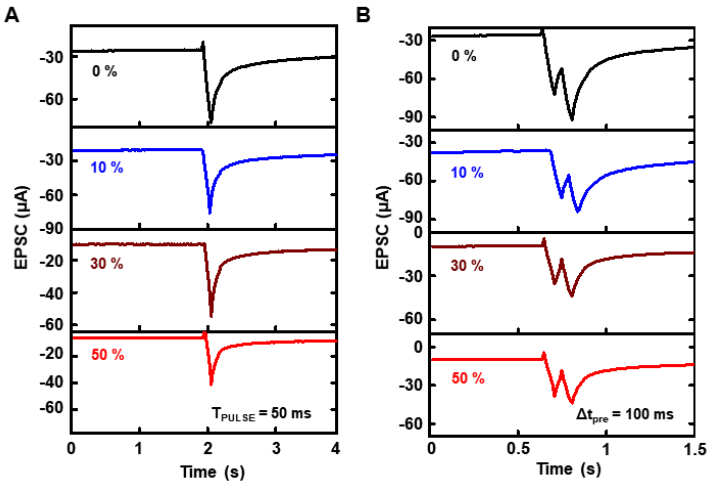

Fig. S7. EPSCs under mechanical strain along the channel width direction. (**A**) Single presynaptic pulse induced EPSC under different levels of mechanical strain. (**B**) The EPSC triggered by two successive presynaptic pulses under different levels of mechanical strain.

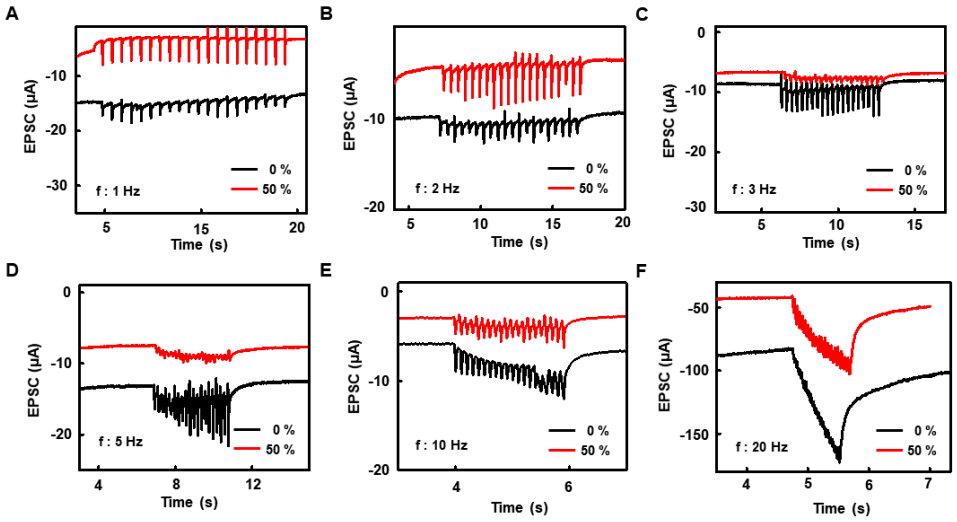

Fig. S8. EPSCs induced by 20 successive presynaptic pulses with different frequencies without (0%) and with 50% strain. (**A**) 1. (**B**) 2. (**C**) 3. (**D**) 5. (**E**) 10. and (**F**) 20 Hz.

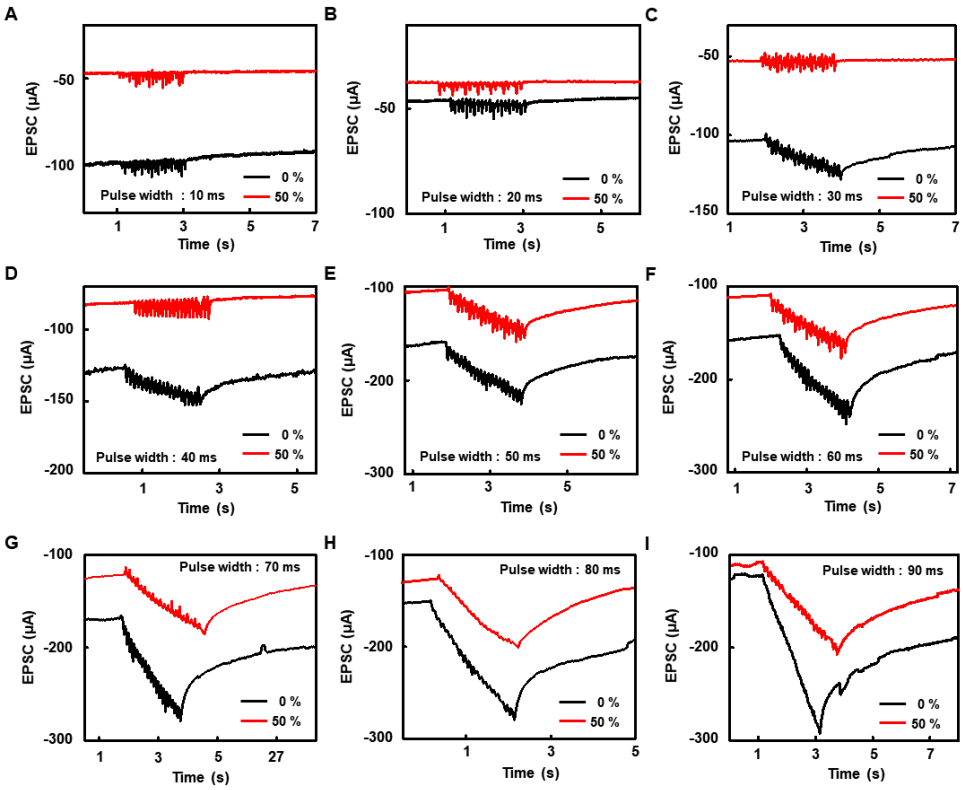

Fig. S9. Memory characteristics from 20 successive presynaptic pulses with different widths without (0%) and with 50% strain. (**A**) 10. (**B**) 20. (**C**) 30. (**D**) 40. (**E**) 50. (**F**) 60. (**G**) 70. (**H**) 80. and (**I**) 90 ms.

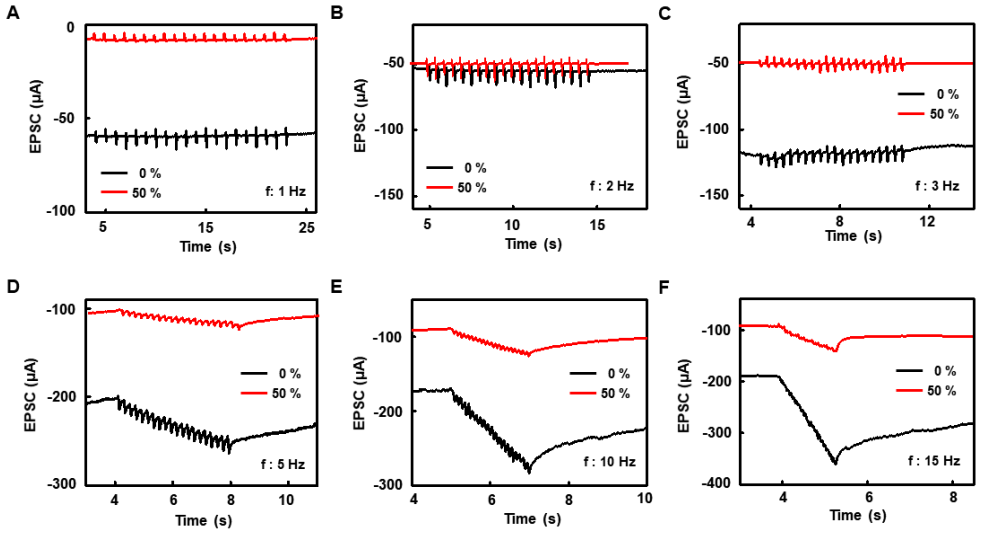

Fig. S10. Memory characteristics with respect to the frequency of presynaptic pulses without (0%) and with 50% strain. (**A**) 1. (**B**) 2. (**C**) 3. (**D**) 5. (**E**) 10. and (**F**) 15 Hz.

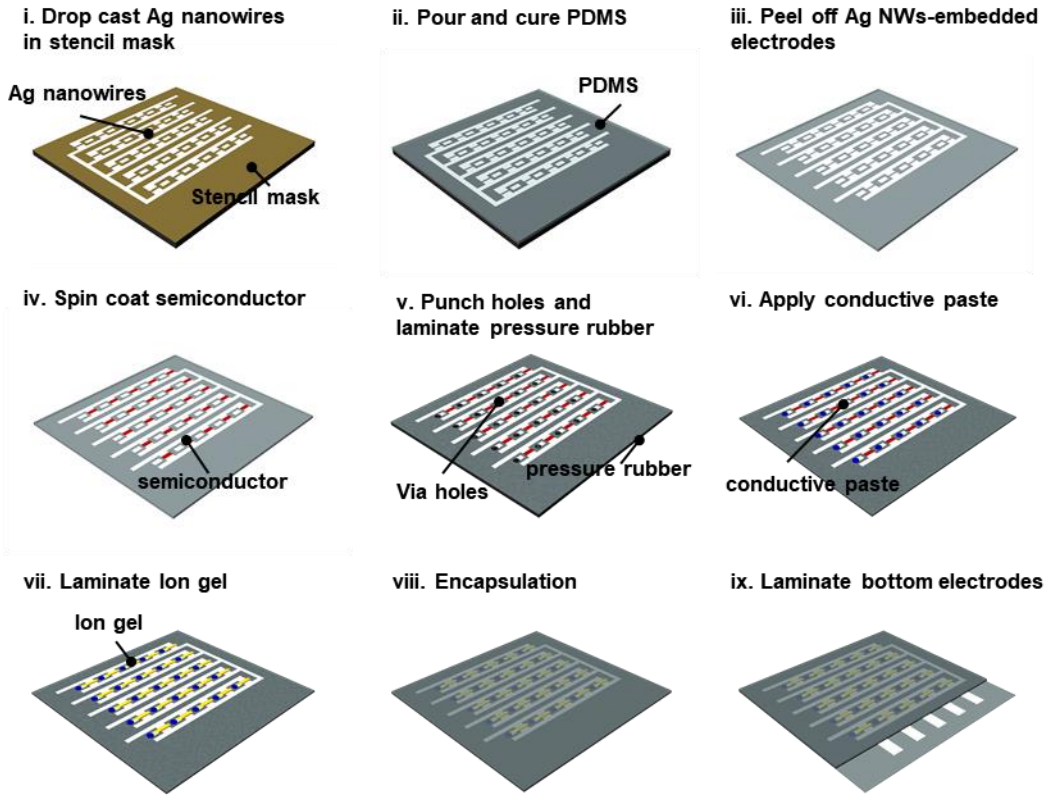

Fig. S11. Schematic illustration of the major fabrication steps for the tactile sensory skin.

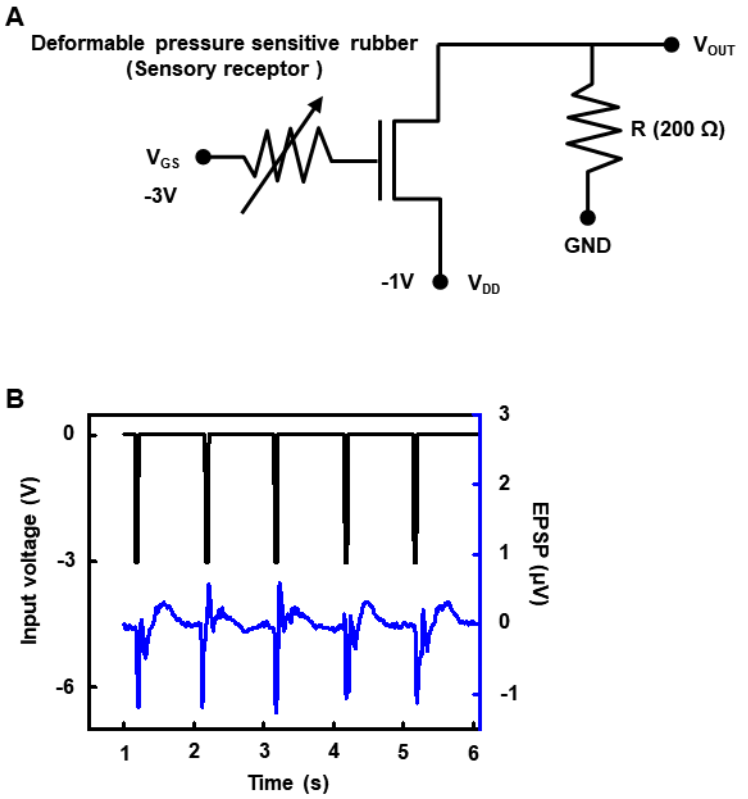

Fig. S12. Neurologically integrated tactile sensory skin. (**A**) Circuit diagram of a single channel. (**B**) Dynamic pulse input from cyclic pressing and releasing and the corresponding EPSP output voltage.

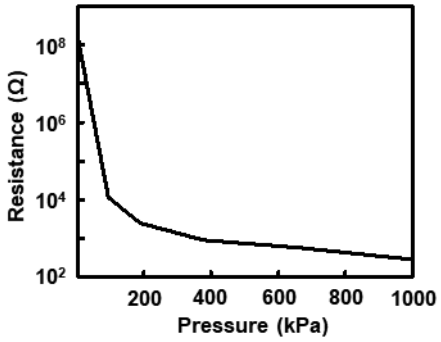

Fig. S13. Resistance change of the pressure-sensitive rubber sheet with respect to the applied pressure.

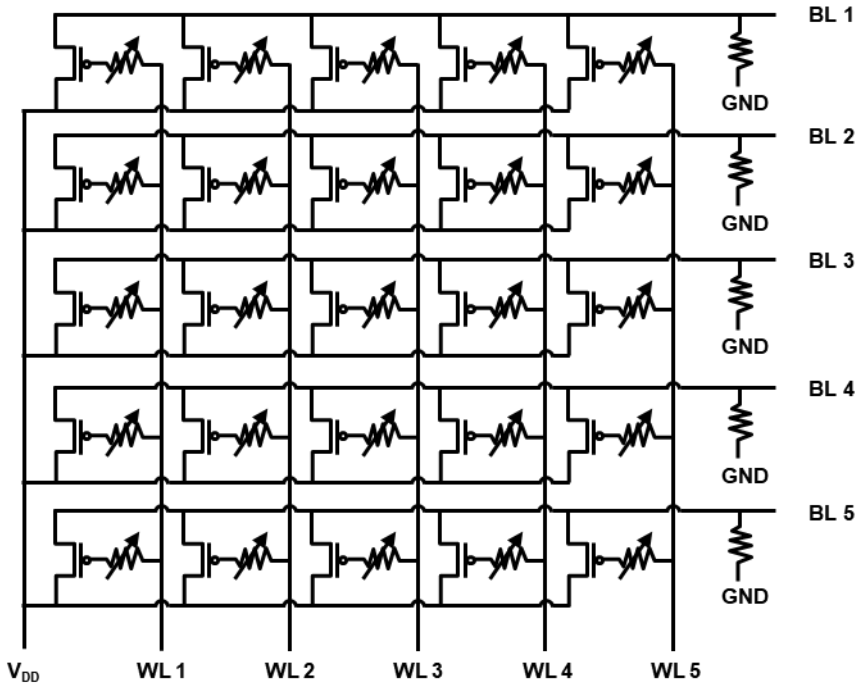

Fig. S14. Circuit diagram of the 5 by 5 arrayed synapse-implemented sensory skin.

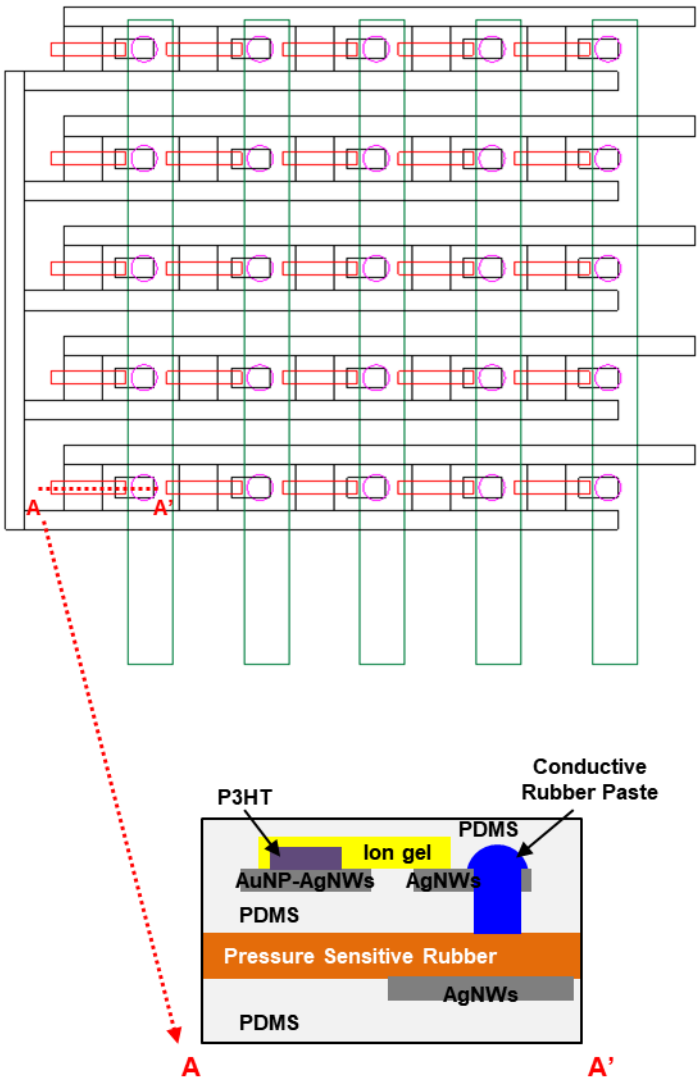

Fig. S15. The schematic geometry and cross-sectional image of the rubbery tactile sensory skin.

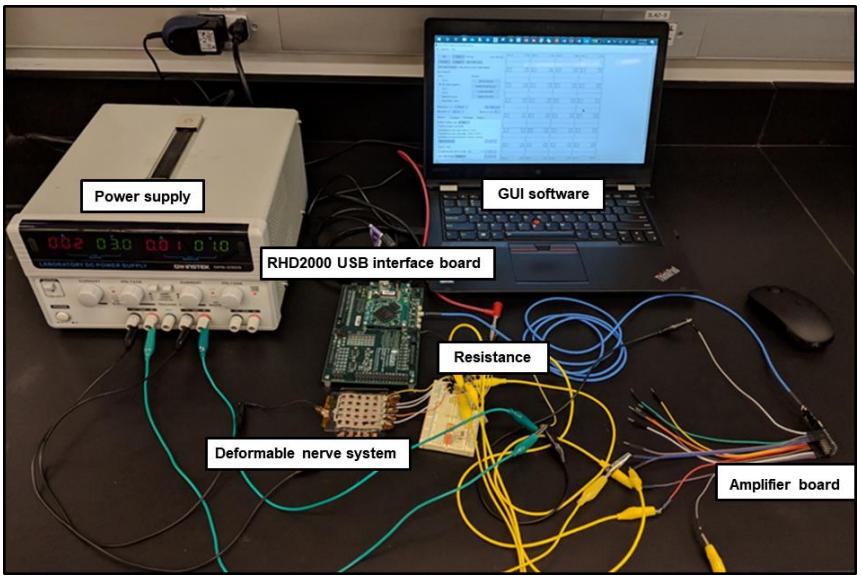

Fig. S16. Measurement setup for EPSP mapping. (Photo Credit: Hyunseok Shim, University of Houston).

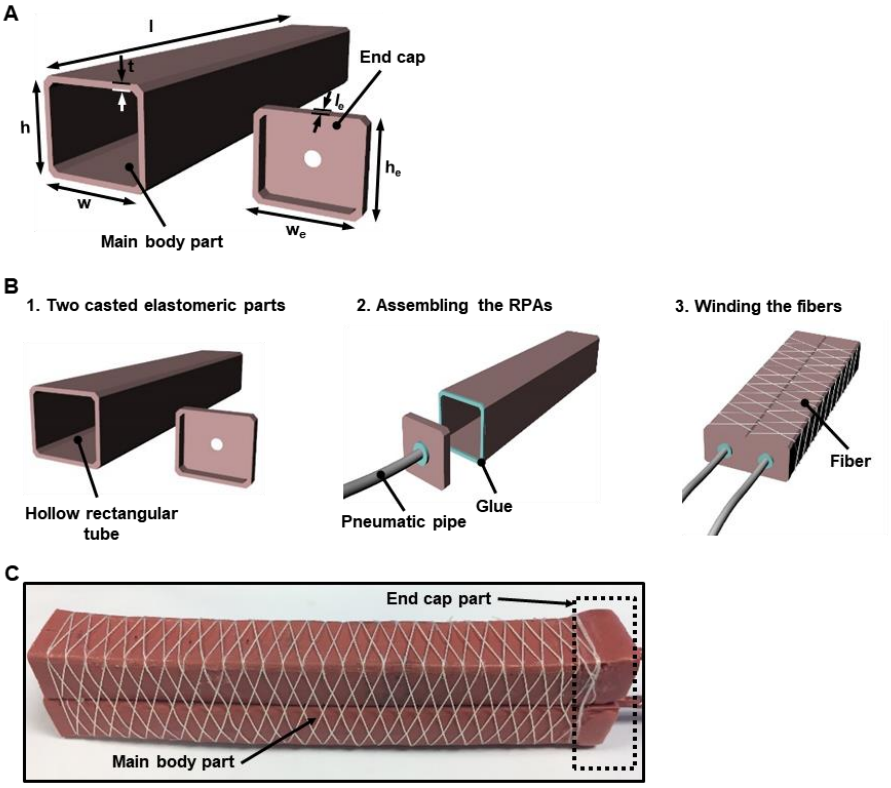

Fig. S17. Design, fabrication, and optical image of soft pneumatic robot. (**A**) The main body part of the RPA has length l = 150 mm, height h = 16 mm, width w = 21 mm, wall thickness t = 2.5 mm. The end cap part of the RPA has length l_e = 4 mm, height h_e = 16 mm, width w_e = 21 mm. (**B**) Schematic illustration of the major fabrication steps for the soft pneumatic robot. (**C**) Optical image of soft pneumatic robot.

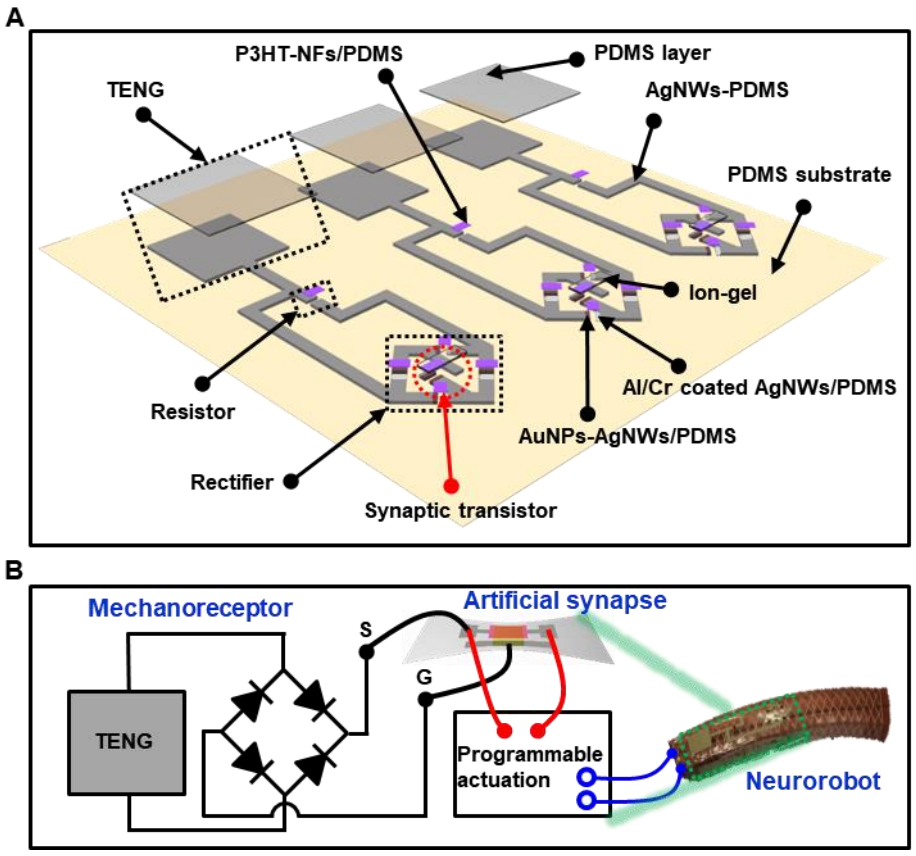

Fig. S18. Synapse-implemented fully rubbery robotic skin. (**A**) An exploded view of the synapse implemented elastic robotic skin. (**B**) Circuit diagram of the robotic skin.

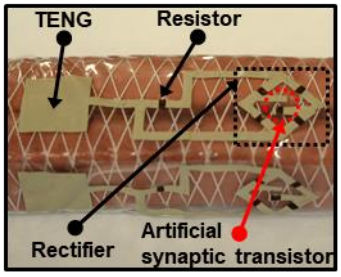

Fig. S19. Optical image of the synapse-enabled elastic robotic skin. (Photo Credit: Hyunseok Shim, University of Houston).

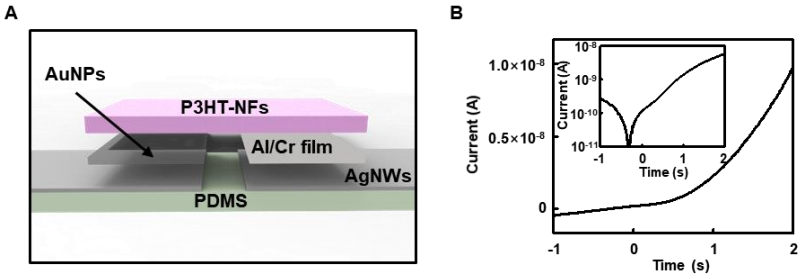

Fig. S20. Schottky diode. (**A**) Schematic structure of the soft Schottky diode. (**B**) I-V curve of the diode.

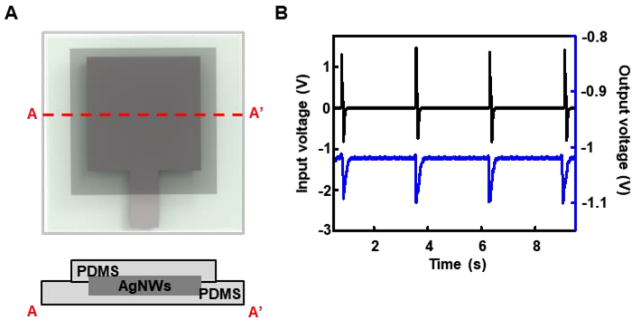

Fig. S21. Triboelectric nanogenerators. (**A**) The schematic layout and cross-sectional image of the TENG. (**B**) The voltage from the TENG before (black) and after (blue) rectification.

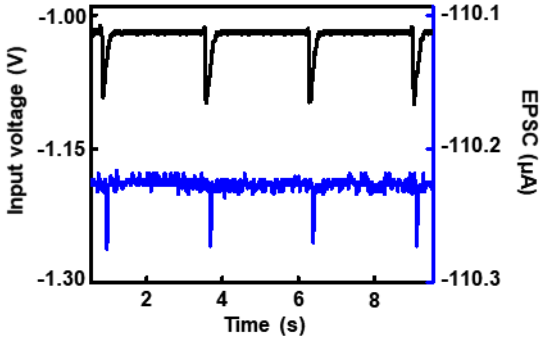

Fig. S22. Input pulse and output EPSC during cyclic tapping.